coatings

MDPI

Article

Structural, Morphologic, and Ferroelectric Properties of PZT Films Deposited through Layer-by-Layer Reactive DC Magnetron Sputtering

Benas Beklešovas [1,*], Aleksandras Iljinas [1], Vytautas Stankus [1], Jurgita Čyvienė [1], Mindaugas Andrulevičius [2], Maksim Ivanov [3] and Jūras Banys [3]

[1] Department of Physics, Kaunas University of Technology, Studentų Str. 50, LT-51368 Kaunas, Lithuania; aleksandras.iljinas@ktu.lt (A.I.); vytautas.stankus@ktu.lt (V.S.); jurgita.cyviene@ktu.lt (J.Č.)
[2] Institute of Materials Science, Kaunas University of Technology, K. Baršausko Str. 59, LT-51423 Kaunas, Lithuania; mindaugas.andrulevicius@ktu.lt
[3] Faculty of Physics, Vilnius University, Sauletekio al. 9, LT-10222 Vilnius, Lithuania; maksim.ivanov@ff.vu.lt (M.I.); juras.banys@ff.vu.lt (J.B.)
* Correspondence: benas.beklesovas@ktu.edu; Tel.: +370-67357976

Abstract: Lead zirconate titanate (PZT) is a widely used material with applications ranging from piezoelectric sensors to developing non-volatile memory devices. $Pb(Zr_xTi_{1-x})O_3$ films were deposited by DC reactive magnetron sputtering at a temperature range of (500–600) °C. X-ray diffraction (XRD) indicated the perovskite phase formation in samples synthesized at 550 °C, which agrees with Raman data analysis. Scanning electron microscopy (SEM) measurements supplemented XRD data and showed the formation of dense PZT microstructures. Further X-ray photoelectron spectroscopy (XPS) analysis confirmed that the Zr/Ti ratio corresponds to the $Pb(Zr_{0.58}Ti_{0.42})O_3$ content. Dielectric measurement of the same sample indicated dielectric permittivity to be around 150 at room temperature, possibly due to the defects in the structure. P-E measurements show ferroelectric behavior at a temperature range of (50–180) °C. It was found that the remnant polarization increased with temperature, and at the same time, coercive field values decreased. Such behavior can be attributed to energetically deep defects.

Keywords: ferroelectric; lead-zirconate titanate; PZT; thin films; magnetron sputtering

Citation: Beklešovas, B.; Iljinas, A.; Stankus, V.; Čyvienė, J.; Andrulevičius, M.; Ivanov, M.; Banys, J. Structural, Morphologic, and Ferroelectric Properties of PZT Films Deposited through Layer-by-Layer Reactive DC Magnetron Sputtering. *Coatings* **2022**, *12*, 717. https://doi.org/10.3390/coatings12060717

Academic Editors: Cecilia Mortalò, Silvia Maria Deambrosis and Valentina Zin

Received: 22 April 2022
Accepted: 20 May 2022
Published: 24 May 2022

1. Introduction

Lead-based ferroelectric materials, such as $PbTiO_3$ (PT), $PbZr_xTi_{1-x}O_3$, La-doped and Nd-doped $Pb(Zr_xTi_{1-x})O_3$ (PLZT), and (PNZT) are widely used in micro- and nanoelectronics [1–3]. Lead zirconate titanate (PZT) currently dominates the market for piezoelectric materials [4–6]. It has appropriate piezoelectric, ferroelectric, and pyroelectric properties for the production of various sensors, actuators, and transducers [1,2,7,8]. Recently, ferroelectric thin films have attracted much attention owing to their photovoltaic properties arising from ferroelectric remnant polarization [9–11]. Because of PZT's electric properties, it can be used in non-volatile random access memory (FRAM) applications as well [12–14]. During practical use, PZT has problems with high coercive field and leakage current, short retention, a tendency to imprint, and fatigue with usual platinum electrodes [15,16]. These properties of PZT thin films depend on substrate materials (lattice parameters and thermal expansion coefficient), the deposition method, film thickness, measurement frequencies used, etc. The deposition conditions, such as deposition rate, composition, and substrate temperature, are very important factors in the growing process of PZT films. Many different chemical and physical deposition techniques are used for PZT film formation: RF magnetron sputtering [17–21], pulsed laser deposition [22–24], sol-gel techniques [9,25,26], chemical vapor deposition [27], etc. During the synthesis of the PZT perovskite phase,

by using these methods, high substrate temperatures are necessary. Often for improving structural and ferroelectric properties, post-annealing at high temperatures (from 700 to 1300 °C depending on the synthesis method) is needed. Film post-annealing is not desirable because, during crystal structure enhancement, cracks and voids are usually obtained [28]. These defects of the surface make PZT films unsuitable for nanoelectronics applications. Methods that allow us to obtain the appropriate structural and morphological properties of PZT films in situ in low temperatures are more desirable. For these reasons, film growth by the reactive magnetron layer-by-layer deposition method in a vacuum is one of the most promising methods for PZT film formation without post annealing. This variation of magnetron sputtering allows us to synthesize large areas of thin films with perovskite structures, uniform thickness, and stoichiometry at relatively low temperatures [29,30]. The DC sputtering from three metallic Pb, Ti, and Zr targets by varying sputtering rate of each cathode provides the opportunity to obtain a wide composition range of $Pb(Zr_xTi_{1-x})O_3$ in Ti rich or Zr rich compositions. In this work PZT films were synthesized directly (in situ) using layer-by-layer reactive DC magnetron sputtering on the platinized silicon substrate. The effects of deposition temperature on the structural, morphological, and ferroelectric properties were investigated.

2. Materials and Methods

PZT films were grown on a platinum-coated silicon substrate using the layer-by-layer reactive DC magnetron deposition method. The substrate consisted of a multilayer ($Pt/Ti/SiO_2/Si$) structure. This structure was based on a crystal Si (100) substrate that was coated with a 1 µm thick silicon oxide layer by a thermal oxidation method and 20 nm titanium and 100 nm platinum bottom electrode layers which were grown by magnetron sputtering. The top Pt layer had a (111) crystallographic orientation. To improve the adhesion of the PZT layer with the substrate and to avoid blistering, a 5 nm thick Ti seeding layer was deposited by reactive magnetron sputtering in the argon gas environment (1.3 Pa) at 750 °C. The PZT layer was formed using three flat magnetrons, each equipped with 3 inches of Ti, Pb, and Zr targets (from Kurt. J. Lesker Company, Jefferson Hills, PA, USA, purity 99.95%). They were aligned to be at the same height, parallel to each other (Figure 1a). The magnetrons were arranged in the line of the sample trajectory. The sample (facing downwards) was held above the magnetrons on the moving heating element. The holder was moving by pendulum principle parallel to the targets (magnetrons), with a constant 0.3 Hz frequency. When the substrate moved above each operating magnetron, a layer of respective oxide atoms was deposited on the substrate. The substrate moving zone was positioned at a 65 mm parallel distance from the targets.

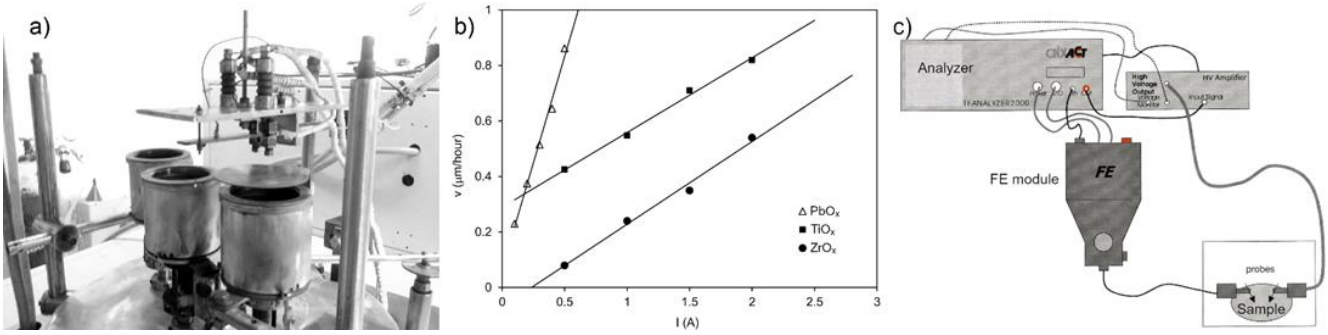

Figure 1. (**a**) Experimental equipment; (**b**) deposition velocity dependence on the magnetron cathode current at the same conditions; (**c**) dielectric properties measurement setup (adapted with permission from Ref. [31]. Copyright 2000, aixACCT Systems GmbH).

The deposition was conducted at 1.33 Pa oxygen pressure on different temperature substrates. Other researchers suggest a temperature range of 500–700 °C, although the formation of secondary phases due to evaporation of lead at higher temperatures was

also reported [32–34]. Thus, the selected temperature range was (500–600 °C) accordingly. The deposition rates were determined after 30 min of synthesis (Figure 1b). Using the formula for the amount of material (1) and deposition rates from Figure 1b, the magnetron parameters for the desired $Pb(Zr_{0.58}Ti_{0.42})O_3$ composition were determined:

$$v = \frac{N}{N_A}, \quad (1)$$

(v—the amount of material (mol); N—the number of molecules; N_A—Avogadro constant (6.02×10^{23} mol^{-1})). For this reason, deposition rates were chosen to be 7 nm/min, 8 nm/min, and 6 nm/min for PbO, TiO_2, and ZrO_2, respectively. Such deposition rates were selected for the formation of PZT composition close to the morphotropic phase boundary (MPB) region. Varying Zr/Ti ratios failed to obtain perovskite phases as a result of the formation of the pyrochlore phase in Ti-rich films [35,36]. The formed film thickness was close to 0.5 micrometer, as reported in other research, which suggests that such thickness can contribute to improving dielectric properties due to tensile stress decrease [37]. PZT layer thickness was measured by a Linnik microinterferometer, profilometer (Ambios XP-200 Profiler, Ambios Technology Inc., Santa Cruz, CA, USA) and using the cross-section SEM view scale. The atomic composition on the surfaces of deposited films was studied using X-ray photoelectron spectroscopy. For the surface composition analysis, a Thermo Scientific ESCALAB 250Xi spectrometer (Thermo Fisher Scientific Inc., Waltham, MA, USA) with monochromatized AlKα radiation (hν = 1486.6 eV) was used. The pressure in the analytical chamber during the measurements was lower than 2×10^{-7} Pa. X-ray spot size for the spectra acquisitions was 0.3 mm. The 40 eV pass energy was used for the spectra acquisition. The energy scale of the system was calibrated according to Au $4f_{7/2}$, Ag $3d_{5/2}$, and Cu $2p_{3/2}$ peaks position. The calculations of atomic concentration were performed using the original ESCALAB 250Xi Avantage software. PZT films were analyzed without the surface cleaning procedure the next day after deposition. The top electrodes used to perform traditional ferroelectric measurements (creating a capacitor structure) were deposited using aluminum thermal evaporation through the mask. The electrode matrix consisted of 5–10 disk-shaped electrodes (thickness 100 nm, surface area 1.23 mm^2). The layer surface was inspected using SEM (RAITH-e-LiNE, Raith GmbH, Dortmund, Germany). The crystallographic structure of films was investigated with XRD equipment (Bruker D8 series diffractometer, Bruker AXS from GmbH, Bruker Corporation, Billerica, MA, USA) using monochromatic Cu Kα radiation with Bragg–Brentano geometry. Polarization dependence on the electric field strength (ferroelectric properties) was measured by means of the Sawyer and Tower method by supplying the created capacitor structure with up to 50 V AC sine voltages. The frequency ranged from 100 Hz to 0.1 MHz (test setup in Figure 1c). For Raman spectroscopy, Spectra-Physics (Spectra-Physics, Inc., Milpitas, CA, USA) with 150 mW laser equipment was used.

3. Results and Discussion

3.1. XRD Analysis

The XRD patterns of the deposited films at 500, 550, and 600 °C substrate temperatures are shown in Figure 2. The best dielectric properties of $Pb(Zr_xTi_{1-x})O_3$ were obtained at x value ~0.58 because the composition was near the morphotropic phase boundary [38]. The crystalline structure of PZT films depends on the substrate temperature when films are synthesized. The selected temperature interval is optimal for in situ perovskite phase formation [18,29]. The samples deposited at substrate temperatures of 500 °C and below show a pyrochlore phase due to low formation energy [28,39]. Deposited at 600 °C temperature, PZT shows no perovskite phase because of the high volatility of lead oxide (at high temperatures); therefore, it results in a lead deficiency in these films.

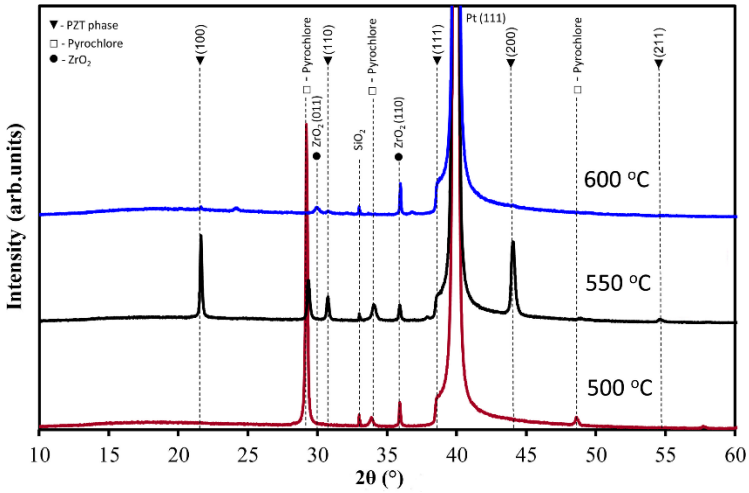

Figure 2. XRD patterns of PZT films deposited at 500, 550, and 600 °C substrate temperature.

The analysis of the crystal structure of the pattern deposited at 550 °C was identified as a rhombohedral space group (R-3 m) nanocrystal PZT oxide phase. The peaks at 2θ = 21.63°, 30.73°, 38.59°, and 44.04° are attributed to the (100), (110), (111), and (200) PZT planes, respectively. Two pyrochlore phase low-intensity peaks are observed at 29.34° and 34.05°, respectively. The highest intensity peak at 2θ = 39.91° corresponds to the bottom electrode of platinum (111) reflection. The peaks at 2θ = 35.91° are attributed to the (110) ZrO_2 plane. A crystallite size of 59 nm of PZT was obtained. It is clear that in this composition, the PZT film exhibits a rhombohedral structure with random orientation.

3.2. Raman Spectra Analysis

Figure 3 show the Raman spectra analysis of the deposited films. At first, the wide scan (100–3000 cm^{-1}) analysis of all samples and substrates without PZT film was performed for the investigation of zones and for the purpose of separating Pt peaks from PZT (due to PZT films transparency to the laser radiation of 532 nm wavelength). Figure 3a clearly show that in the 1000–3000 cm^{-1} zone, there were only Pt peaks; therefore, it was decided to investigate the peaks only in the 100–1000 cm^{-1} zone. In Figure 3b, a narrow spectra zone is seen, where three peaks (126, 804 and 828 cm^{-1}) are attributed to Pt (RRUFF™ database). All other peaks marked X should correspond to different $Pb(Zr_xTi_{1-x})O_y$ film phases.

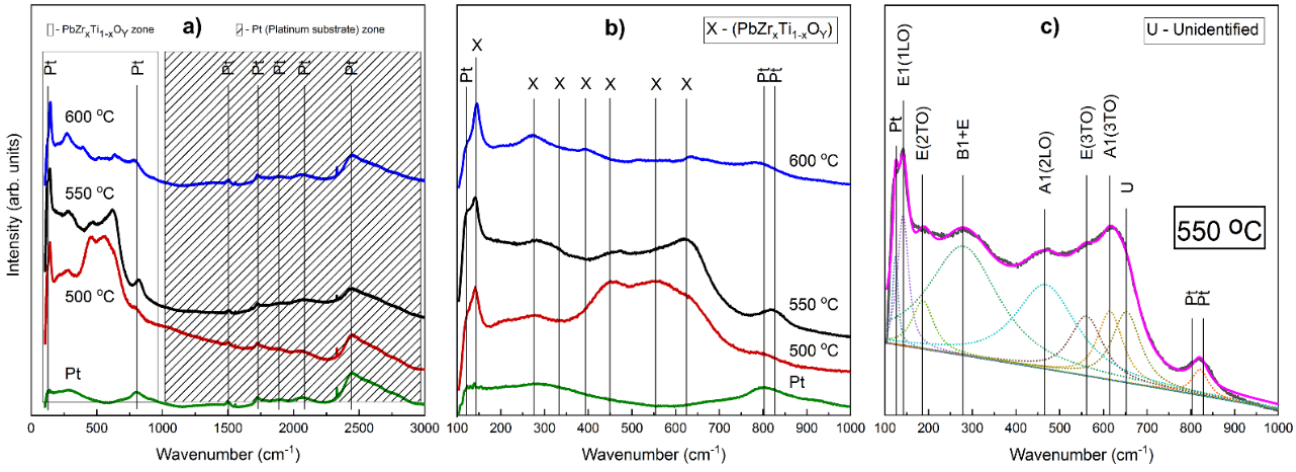

Figure 3. Raman spectra of PZT thin films deposited at 500, 550 and 600 °C temperatures and substrate ($Pt/Ti/SiO_2/Si$). (**a**) Wide-scan spectra; (**b**) narrow; (**c**) fitted spectrum of the film deposited at 550 °C temperature.

Based on the XRD analysis in the previous section, the fitting of film, which exhibits a rhombohedral structure (deposited at 550 °C), was carried out. The fitting in Figure 3c identified 142, 183, 276, 472, 561, and 613 peaks. The Raman modes for the PZT ferroelectrical structure at the morphotropic phase boundary (MPB) are located at around 138, 154, 210, 227, 270, 340, 430, 477, 520, 560, 710, and 790 cm^{-1}. Such modes are identified as E(1LO), A1(1TO), A1(1LO), E(2TO), B1+E, A1(2TO), E1(2LO), A1(2LO), E(3TO), A1(3TO), E(3LO), and A1(3LO), respectively [40–42]. Therefore, the founded modes in Figure 3c can be attributed to E(1LO), E(2TO), B1+E, A1(2LO), E(3TO), and A1(3TO). This fact confirms our presumption of the formation of the ferroelectric PZT phase at 550 °C deposition temperature.

3.3. SEM Analysis

The microstructure images of PZT synthesized at a temperature range of (500–600) °C are shown in Figure 4a–c. According to XRD and P-E measurements, the perovskite phase formed at 550 °C synthesis temperature is seen in Figure 4b. The obtained structure is dense with minimal porosity. Other structures can also be seen through it. These voids and cracks (marked by white arrows) at the grain boundary could be attributed to the total energy reduction of the system due to strain as the film grows thicker. Other reasons for voids could be related to the nucleation sites. The average grain size of PZT was ~250 nm. Other structures underneath the PZT (Figure 4b) can be attributed to the pyrochlore which was formed at the start of the synthesis when the substrate temperature was higher after the Ti seeding layer formation. Figure 4a supplement XRD data, which shows mainly the pyrochlore phase formation at the synthesis temperature of 500 °C. The same structures are represented in Figure 4b through PZT gaps. Increasing the synthesis temperature to 600 °C results in the lead loss due to volatilization (Figure 4c). The disproportion of stoichiometry components leads to the formation of ZrO_2 and other phases, where different microstructures compared to Figure 4a,b were obtained.

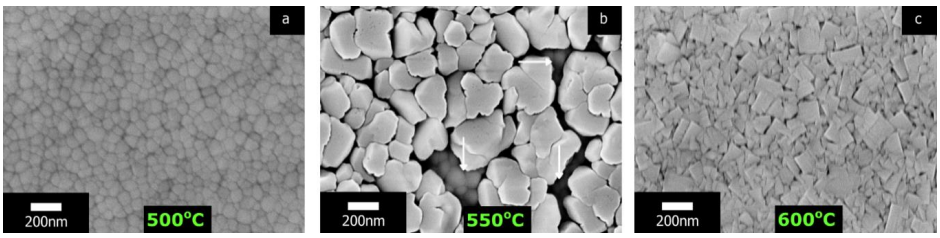

Figure 4. SEM images of films deposited at (**a**) 500 °C; (**b**) 550 °C; (**c**) 600 °C substrate temperatures.

The cross-section view of PZT film deposited at 550 °C is displayed in Figure 5. It shows a dense formation of the film with vertical shadows, which indicate the column growth. The columns are uniform, with no visible embedded pyrochlore structures; thus, they can be formed at the PZT/Pt interface, as seen in Figure 4b. The film thickness reaches ~500 nm, which agrees with the measurements by the profilometer.

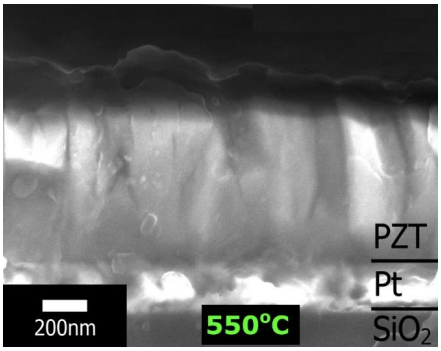

Figure 5. Cross-section of film deposited at 550 °C substrate temperature.

3.4. XPS Analysis

The atomic composition of the films was studied using X-ray photoelectron spectroscopy (XPS). Figure 6 demonstrate wide-scan spectra in the binding energy range of 0–1000 eV of XPS analysis of PZT thin films formed at 550 °C substrate temperature. In this figure, Pb 4f, Zr 3d, Ti 2p, O 1s, and C 1s peaks are shown. Some other peaks are present in the spectra due to the contamination which occurred during the deposition or analysis processes. In our case, the obtained carbon concentration at the surface amounted to 51%. Carbon C 1s at 285 eV and an additional O 1s peak at 532 eV were attributed to carbon contamination [43].

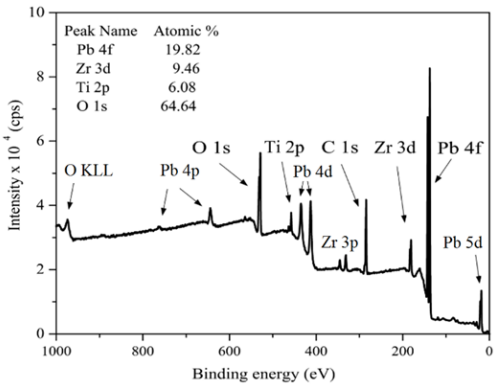

Figure 6. Wide-scan XPS spectra of the deposited at 550 °C substrate temperature PZT films.

The narrow-scanning XPS spectra of the Pb 4f, Zr 3d, Ti 2p, and O 1s peaks are shown in Figure 7a–d, respectively. The Pb 4f doublets consist of two clearly separated peaks of Pb $4f_{7/2}$ at 137.5 and Pb4 $f_{5/2}$ at 142.35 eV, respectively, as shown in Figure 7a. The Zr 3d spin-orbit doublets consist of two separated peaks of $3d_{3/2}$ at 183.18 and $3d_{5/2}$ at 180.81 eV, as shown in Figure 7b. The Ti 2p doublets consist of two separated peaks of $2p_{1/2}$ at 463.37 and $2p_{3/2}$ at 457.62 eV and are shown in Figure 7c. The O 1s fitted spectrum consists of three peaks of O 1s at 531.94, 530.54, and 529.07 eV, as shown in Figure 7d. The peak position and the spin-orbit splitting between them are in accordance with the values reported for PZT [43–46]. From the Zr/Ti ratio, we determined that our film has the $Pb(Zr_{0.58}Ti_{0.42})O_3$ composition. The results showed that the zirconium content was higher in the PZT layer formed at 500 °C and lower at 600 °C than at 550 °C. The titanium fraction in the PZT coating was the opposite.

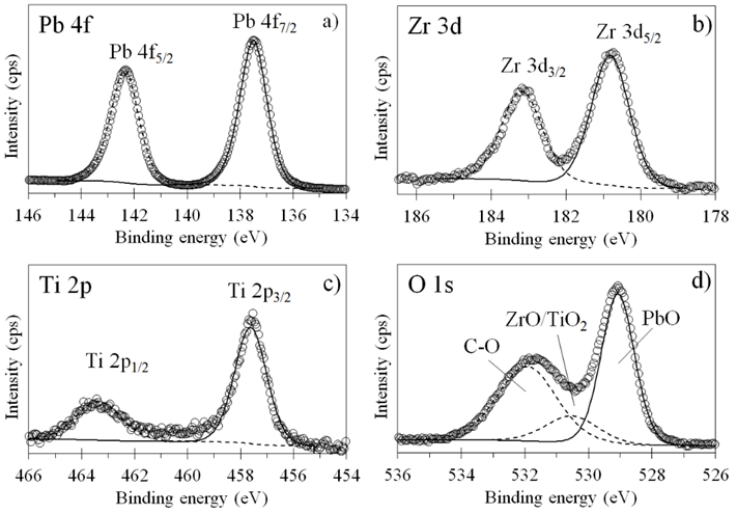

Figure 7. High-resolution XPS spectra deconvolution for the (**a**) Pb 4f; (**b**) Zr 3d; (**c**) Ti 2p; (**d**) O 1s regions of the PZT thin films deposited at 550 °C substrate temperature.

3.5. Analysis of Dielectric Properties

Dielectric properties of PZT films were measured from 20 Hz up to 100 kHz during the cooling cycle at a 1 K/min cooling rate using an LCR meter Agilent /HP4284 A (Agilent Technologies, Inc., Santa Clara, CA, USA). Dielectric hysteresis was obtained using an aixACCT TF Analyzer 2000 E system (aixACCT Systems GmbH, Aachen, Germany). Temperature dependences of the real part of dielectric permittivity (Figure 8) show minor variation. High dielectric losses were observed at higher temperatures implying that our samples are slightly conductive.

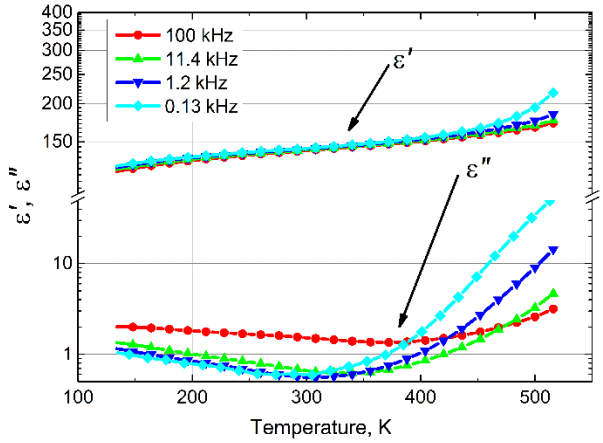

Figure 8. Real and imaginary parts of the dielectric permittivity of PZT film as a function of temperature.

Furthermore, dielectric losses slightly increase as temperature decreases. This can indicate that we have a glass-like dielectric anomaly at lower temperatures. The underlying microscopic origin can be related to a number of defects in the system. A defective structure can also explain why, at room temperature, our sample has a relatively low dielectric permittivity, which is around 150 (typically 1000 is observed) [47].

The ferroelectric hysteresis loops of PZT film are shown in Figure 9a. First of all, they show a banana-like shape [48], which indicates a rather high conductivity. This fact complements our dielectric measurements. However, it was still possible to estimate the real hysteresis loop by taking into account the specimen's resistivity and capacitance to compensate for their contribution to experimental loops (Figure 9b).

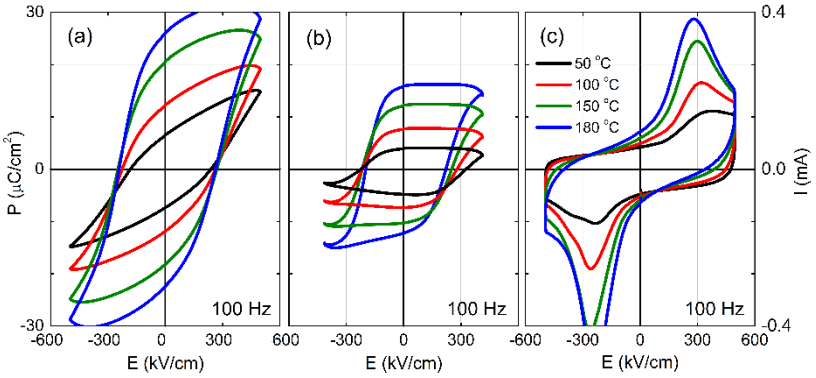

Figure 9. (**a**) Measured; (**b**) compensated dielectric hysteresis of PZT films; (**c**) current dependence of PZT film films as a function of the electrical field.

Both experimental and calculated loops exhibit typical behavior: the value of polarization grows as the temperature increases. This can be explained by a wide distribution of coercive fields. This phenomenon exists due to the domain friction effect [49]. An increase in temperature leads to domain friction decrease; therefore, there are more domains that are more oriented in one direction. Additionally, logically, a less coercive field is needed [50].

This means that at higher temperatures, a bigger fraction of domains can be switched, leading to a higher switchable polarization. This is confirmed by the switching currents (Figure 9c): some switching is observable in all cases, but the current peaks are higher at higher temperatures. Furthermore, they clearly shift to lower fields as the material is heated. The observed effective coercive field is quite large, well above the bulk value of 20 kV/cm in the case of hard (Nb-doped) PZT ceramics [47]. Moreover, in Figure 9c, we can see that peaks of switching currents are of a different magnitude and positive peaks are smaller than the negative ones. These facts, together with a wide distribution of coercive fields, can only be explained by a high concentration of energetically deep defects, which pin the domain walls, thus impeding their movement during the switching process. Ferroelectric hysteresis loops of PZT film were not obtained when the substrate temperature was 500 °C and 600 °C during the PZT formation process.

4. Conclusions

$Pb(Zr_{0.58}Ti_{0.42})O_3$ films were formed using the DC reactive magnetron sputtering layer-by-layer method at a temperature range of (500–600) °C. XRD data indicated perovskite formation at 550 °C substrate temperature, which was supplemented by Raman spectroscopy. The pyrochlore phase was formed due to low formation energy at a lower synthesis temperature (500 °C). Lead volatilization occurred at a higher synthesis temperature (600 °C). SEM images and supplement of XRD data show the formation of dense perovskite microstructures at 550 °C. XPS analysis of the sample synthesized at 550 °C confirmed that the Zr/Ti ratio corresponds to $Pb(Zr_{0.58}Ti_{0.42})O_3$ content. Further dielectric analysis showed slight conduction at higher as well as at lower than room temperatures. At higher temperatures, the larger fraction of domains can be switched; the measurements are supplemented by current dependence on the applied electric field strength. It was observed that the current peaks are higher at higher temperatures, and that can be explained as a result of the occurrence of energetically deep defects.

Author Contributions: Conceptualization, A.I. and V.S.; methodology, V.S.; formal analysis, A.I. and V.S.; investigation, B.B., V.S., J.Č., M.A., M.I., and J.B.; resources, V.S.; writing—original draft preparation, B.B., A.I., V.S., M.A., and J.Č.; visualization, V.S.; supervision, V.S.; project administration, A.I. All authors have read and agreed to the published version of the manuscript.

Funding: This research received no external funding.

Institutional Review Board Statement: Not applicable.

Informed Consent Statement: Not applicable.

Data Availability Statement: The authors confirm that the data supporting the findings of this study are available within the article.

Conflicts of Interest: The authors declare no conflict of interest.

References

1. Zhou, Q.; Lau, S.; Wu, D.; Shung, K.K. Piezoelectric films for high frequency ultrasonic transducers in biomedical applications. *Prog. Mater. Sci.* **2011**, *56*, 139–174. [CrossRef] [PubMed]
2. Zribi, A.; Fortin, J.B. *Functional Thin Films and Nanostructures for Sensorssynthesis, Physics and Applications*; Springer: New York, NY, USA, 2009.
3. Steinem, C.; Janshoff, A. *Piezoelectric Sensors*; Springer: Berlin/Heidelberg, Germany, 2007.
4. Gao, W.; Zhu, Y.; Wang, Y.; Yuan, G.; Liu, J.-M. A review of flexible perovskite oxide ferroelectric films and their application. *J. Materiomics* **2020**, *6*, 1–16. [CrossRef]
5. Sezer, N.; Koç, M. A comprehensive review on the state-of-the-art of piezoelectric energy harvesting. *Nano Energy* **2020**, *80*, 105567. [CrossRef]
6. Ryndzionek, R.; Sienkiewicz, Ł. A review of recent advances in the single- and multi-degree-of-freedom ultrasonic piezoelectric motors. *Ultrasonics* **2021**, *116*, 106471. [CrossRef]
7. Fei, C.; Chen, Z.; Fong, W.M.; Zhu, B.; Wang, L.; Ren, W.; Li, Y.; Shi, J.; Shung, K.K.; Zhou, Q. Modification of microstructure on PZT films for ultrahigh frequency transducer. *Ceram. Int.* **2015**, *41*, S650–S655. [CrossRef]

8. Wixom, A.S.; Anderson, M.J.; Bahr, D.F.; Morris, D.J. A new acoustic transducer with a pressure-deformed piezoelectric diaphragm. *Sens. Actuators A Phys.* **2012**, *179*, 204–210. [CrossRef]
9. Anoop, G.; Seo, J.; Han, C.J.; Lee, H.J.; Kim, G.W.; Lee, S.S.; Park, E.Y.; Jo, J.Y. Ultra-thin platinum interfacial layer assisted-photovoltaic response of transparent Pb(Zr,Ti)O 3 thin film capacitors. *Sol. Energy* **2015**, *111*, 118–124. [CrossRef]
10. Gupta, R.; Gupta, V.; Tomar, M. Ferroelectric PZT thin films for photovoltaic application. *Mater. Sci. Semicond. Process.* **2019**, *105*, 104723. [CrossRef]
11. Chen, M.; Shen, X.; Zhou, C.; Cao, D.; Xue, W. High-performance self-powered visible-blind ultraviolet photodetection achieved by ferroelectric PbZr0.52Ti0.48O3 thin films. *J. Alloy Compd.* **2021**, *897*, 163208. [CrossRef]
12. Bez, R.; Pirovano, A. 1—Overview of non-volatile memory technology: Markets, technologies and trends. In *Advances in Non-Volatile Memory and Storage Technology*; Nishi, Y., Ed.; Woodhead Publishing: Sawston, UK, 2014; pp. 1–24.
13. Eshita, T.; Tamura, T.; Arimoto, Y. 14—Ferroelectric random access memory (FRAM) devices. In *Advances in Non-Volatile Memory and Storage Technology, Nishi, Y., Ed.*; Woodhead Publishing: Sawston, UK, 2014; pp. 434–454.
14. Mao, D.; Mejia, I.; Salas-Villasenor, A.; Singh, M.; Stiegler, H.; Gnade, B.; Quevedo-Lopez, M. Ferroelectric random access memory based on one-transistor–one-capacitor structure for flexible electronics. *Org. Electron.* **2013**, *14*, 505–510. [CrossRef]
15. Liu, G.; Zhang, S.; Jiang, W.; Cao, W. Losses in ferroelectric materials. *Mater. Sci. Eng. R Rep.* **2015**, *89*, 1–48. [CrossRef] [PubMed]
16. Genenko, Y.; Glaum, J.; Hoffmann, M.J.; Albe, K. Mechanisms of aging and fatigue in ferroelectrics. *Mater. Sci. Eng. B* **2015**, *192*, 52–82. [CrossRef]
17. Wang, Z.; Lai, Z.; Hu, Z. Low-temperature preparation and characterization of the PZT ferroelectric thin films sputtered on FTO glass substrate. *J. Alloy Compd.* **2013**, *583*, 452–454. [CrossRef]
18. Bose, A.; Maity, T.; Bysakh, S.; Seal, A.; Sen, S. Influence of plasma pressure on the growth characteristics and ferroelectric properties of sputter-deposited PZT thin films. *Appl. Surf. Sci.* **2010**, *256*, 6205–6212. [CrossRef]
19. Bose, A.; Sreemany, M.; Bysakh, S. Influence of processing parameters on the growth characteristics and ferroelectric properties of sputtered PZT thin films on stainless steel substrates. *Appl. Surf. Sci.* **2013**, *282*, 202–210. [CrossRef]
20. Sreemany, M.; Bose, A.; Sen, S. Influence of chemical composition, phase and thickness of TiOx ($x \leq 2$) seed layer on the growth and orientation of the perovskite phase in sputtered PZT thin films. *Mater. Chem. Phys.* **2009**, *115*, 453–462. [CrossRef]
21. Maurya, K.; Halder, S.; Sen, S.; Bose, A.; Bysakh, S. High resolution X-ray and electron microscopy characterization of PZT thin films prepared by RF magnetron sputtering. *Appl. Surf. Sci.* **2014**, *313*, 196–206. [CrossRef]
22. Borowiak, A.; Niu, G.; Pillard, V.; Agnus, G.; Lecoeur, P.; Albertini, D.; Baboux, N.; Gautier, B.; Vilquin, B. Pulsed laser deposition of epitaxial ferroelectric Pb(Zr,Ti)O3 films on silicon substrates. *Thin Solid Films* **2012**, *520*, 4604–4607. [CrossRef]
23. Pham, M.T.; Boukamp, B.; Bouwmeester, H.; Blank, D. Microstructural and electrical properties of nanocomposite PZT/Pt thin films made by pulsed laser deposition. *Ceram. Int.* **2004**, *30*, 1499–1503. [CrossRef]
24. Lin, Y.; Chuang, H.; Shen, J. PZT thin film preparation by pulsed DC magnetron sputtering. *Vacuum* **2009**, *83*, 921–926. [CrossRef]
25. Shakeri, A.; Abdizadeh, H.; Golobostanfard, M.R. Synthesis and characterization of thick PZT films via sol–gel dip coating method. *Appl. Surf. Sci.* **2014**, *314*, 711–719. [CrossRef]
26. Wang, D.; Chen, C.; Ma, J.; Liu, T. Lead-based titanate ferroelectric thin films fabricated by a sol–gel technique. *Appl. Surf. Sci.* **2008**, *255*, 1637–1645. [CrossRef]
27. Moon, J.-W.; Wakiya, N.; Fujito, K.; Iimori, N.; Kiguchi, T.; Yoshioka, T.; Tanaka, J.; Shinozaki, K. Effect of SrTiO3 seed layer deposition time and thickness on low-temperature crystallization and electrical properties of Pb(Zr, Ti)O3 films by metalorganic chemical vapor deposition. *Mater. Sci. Eng. B* **2008**, *148*, 22–25. [CrossRef]
28. Stankus, V.; Dudonis, J.; Pranevicius, L.; Pranevičius, L.L.; Milcius, D.; Templier, C.; Riviere, J.P. On the mechanism of synthesis of PbTiO3 thin films by thermal annealing of Pb/Ti layers in air at atmospheric pressure. *Thin Solid Films* **2003**, *426*, 78–84. [CrossRef]
29. Iljinas, A.; Stankus, V.; Čyvienė, J.; Abakevičienė, B. Formation of PbTiO3 thin films on seed layers using DC magnetron layer-by-layer deposition. *Vacuum* **2015**, *122*, 310–313. [CrossRef]
30. Iljinas, A.; Stankus, V. Structural and ferroelectric properties of bismuth ferrite thin films deposited by direct current reactive magnetron sputtering. *Thin Solid Films* **2016**, *601*, 106–110. [CrossRef]
31. *TF Analyzer 2000 Hysteresis Software*, Ed. 2.2.; aixACCT Systems GmbH: Aachen, Germany, 2013.
32. Velu, G.; Remiens, D. In situ deposition of sputtered PZT films: Control of the growth temperature by the sputtered lead flux. *Vacuum* **2000**, *56*, 199–204. [CrossRef]
33. Kratzer, M.; Castaldi, L.; Heinz, B.; Mamazza, R.; Kaden, D.; Quenzer, H.J.; Wagner, B. In-situ large scale deposition of PZT films by RF magnetron sputtering. In Proceedings of the 2011 International Symposium on Applications of Ferroelectrics (ISAF/PFM) and 2011 International Symposium on Piezoresponse Force Microscopy and Nanoscale Phenomena in Polar Materials, Vancouver, BC, Canada, 24–27 July 2011; pp. 1–4.
34. Park, C.-H.; Son, Y.-G.; Won, M.-S. Microstructure and ferroelectric properties of r.f. magnetron sputtering derived PZT thin films deposited on interlayer (PbO/TiO2). *Microchem. J.* **2005**, *80*, 201–206. [CrossRef]
35. Wang, Z.J.; Aoki, Y.; Kokawa, H.; Ichiki, M.; Maeda, R. Effect of Zr/Ti Ratio on Microstructure and Electrical Properties of Lead Zirconate Titanate Thin Films Derived by Pulsed Laser Deposition. *J. Electroceramics* **2004**, *13*, 41–45. [CrossRef]
36. Khaenamkaew, P.; Muensit, S.; Bdikin, I.; Kholkin, A. Effect of Zr/Ti ratio on the microstructure and ferroelectric properties of lead zirconate titanate thin films. *Mater. Chem. Phys.* **2007**, *102*, 159–164. [CrossRef]

37. Nguyen, M.D.; Dekkers, M.; Vu, H.N.; Rijnders, G. Film-thickness and composition dependence of epitaxial thin-film PZT-based mass-sensors. *Sens. Actuators A Phys.* **2013**, *199*, 98–105. [CrossRef]
38. Zhang, Q.; Cordova, S.; Marshall, J.M.; Shaw, C.P.; Whatmore, R.W. Stress-induced phase formation of PZT 52/48 thin films. *Integr. Ferroelectr.* **2007**, *88*, 85–92. [CrossRef]
39. Iljinas, A.; Marcinauskas, L.; Stankus, V. In situ deposition of PbTiO3 thin films by direct current reactive magnetron sputtering. *Appl. Surf. Sci.* **2016**, *381*, 6–11. [CrossRef]
40. Hu, X.-P.; Duan, D.-W.; Zhang, K.; Zhang, Y.-C.; Chu, S.-Q.; Zhang, J.; Xie, Y.-N.; Guo, D.; Cao, J.-L. Influences of the Amorphous Phase on Local Structures and Properties of Ferroelectric Thin Films. *Ferroelectrics* **2013**, *453*, 149–155. [CrossRef]
41. Rodríguez-Aranda, M.C.; Calderón-Piñar, F.; Espinoza-Beltrán, F.J.; Flores-Ruiz, F.J.; León-Sarabia, E.; Mayén-Mondragón, R.; Yáñez-Limón, J.M. Ferroelectric hysteresis and improved fatigue of PZT (53/47) films fabricated by a simplified sol–gel acetic-acid route. *J. Mater. Sci. Mater. Electron.* **2014**, *25*, 4806–4813. [CrossRef]
42. Rouquette, J.; Haines, J.; Bornand, V.; Pintard, M.; Papet, P.; Sauvajol, J.L. Use of resonance Raman spectroscopy to study the phase diagram ofPbZr0.52Ti0.48O3. *Phys. Rev. B* **2006**, *73*, 224118. [CrossRef]
43. Ştoflea, L.E.; Apostol, N.G.; Trupină, L.; Teodorescu, C.M. Selective adsorption of contaminants on Pb(Zr,Ti)O3 surfaces shown by X-ray photoelectron spectroscopy. *J. Mater. Chem. A* **2014**, *2*, 14386–14392. [CrossRef]
44. Apostol, N.G.; Stoflea, L.E.; Lungu, G.A.; Tache, C.A.; Popescu, D.G.; Pintilie, L.; Teodorescu, C.M. Band bending at free Pb(Zr,Ti)O3 surfaces analyzed by X-ray photoelectron spectroscopy. *Mater. Sci. Eng. B* **2013**, *178*, 1317–1322. [CrossRef]
45. Popescu, D.G.; Huşanu, M.A.; Trupină, L.; Hrib, L.; Pintilie, L.; Barinov, A.; Lizzit, S.; Lacovig, P.; Teodorescu, C.M. Spectro-microscopic photoemission evidence of charge uncompensated areas in Pb(Zr,Ti)O_3(001) layers. *Phys. Chem. Chem. Phys.* **2014**, *17*, 509–520. [CrossRef]
46. Stoflea, L.E.; Apostol, N.G.; Chirila, C.; Trupina, L.; Negrea, R.; Pintilie, L.; Teodorescu, C.M. Schottky barrier versus surface ferroelectric depolarization at Cu/Pb(Zr, Ti)O3 interfaces. *J. Mater. Sci.* **2014**, *49*, 3337–3351. [CrossRef]
47. Randall, C.A.; Kim, N.; Kucera, J.-P.; Cao, W.; Shrout, T.R. Intrinsic and Extrinsic Size Effects in Fine-Grained Morphotropic-Phase-Boundary Lead Zirconate Titanate Ceramics. *J. Am. Ceram. Soc.* **2005**, *81*, 677–688. [CrossRef]
48. Scott, J.F. Ferroelectrics go bananas. *J. Phys. Condens. Matter* **2007**, *20*. [CrossRef]
49. Zarycka, A.; Ilczuk, J.; Chrobak, A. Internal friction related to the mobility of domain walls in sol-gel derived PZT ceramics. *Mater. Sci. Pol.* **2005**, *23*, 159–165.
50. Yimnirun, R.; Wongmaneerung, R.; Wongsaenmai, S.; Ngamjarurojana, A.; Ananta, S.; Laosiritaworn, Y. Temperature scaling of dynamic hysteresis in soft lead zirconate titanate bulk ceramic. *Appl. Phys. Lett.* **2007**, *90*, 112906. [CrossRef]